

# Improving Coherence in Distributed MISO Communication Systems with Local Accelerometer Measurements

D. Richard Brown III and Radu David  
 Worcester Polytechnic Institute  
 100 Institute Rd, Worcester, MA 01609  
 Email: {drb,radud}@wpi.edu

Pat Bidigare  
 Raytheon BBN Technologies  
 Arlington, VA 22207  
 Email: bidigare@ieee.org

**Abstract**—This paper considers a distributed multi-input single-output (MISO) communication system with two or more transmit nodes and a single receive node. Each transmit node has an independent local oscillator and independent kinematics. The receive node periodically estimates the combined time offset and propagation delay of each transmit node and provides feedback to the transmit nodes to facilitate channel tracking and prediction for coherent transmission and passband signal alignment. In addition to the periodic time offset feedback, each receive node also observes periodic measurements from a local accelerometer and uses these measurements to improve the tracking performance. Continuous-time and discrete-time models are developed for a system with one-dimensional kinematics. Numerical results show that local accelerometer measurements can significantly improve the performance of time offset tracking, consequently improving coherence for distributed transmit beamforming and distributed transmit nullforming and also potentially allowing for reduced feedback rates with respect to the conventional receiver-coordinated feedback-only approach.

**Index Terms**—distributed transmission, channel tracking, synchronization, oscillator dynamics, kinematic compensation

## I. INTRODUCTION

We consider the distributed multi-input single-output (MISO) communication scenario in Fig. 1 where a transmission cluster with  $N$  transmit nodes communicates with a single receive node. The transmit cluster transmits as a virtual antenna array and uses coherent transmission techniques, e.g., distributed transmit beamforming [1]–[5] or distributed transmit nullforming [6]–[8]. We assume each node in the system has an independent local oscillator and that no exogenous synchronization signals are present. The receiver facilitates coherent transmission by estimating the combined time offsets and propagation delays and by providing periodic feedback to the transmit nodes.

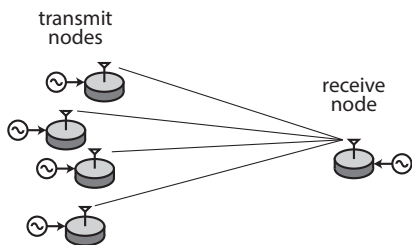


Fig. 1. Distributed MISO system model with  $N$  transmit nodes and one receive node. Each node possesses a single antenna and an independent oscillator.

Since each node in the distributed transmission system has an independent local oscillator and may experience independent kinematic effects, the time offset and propagation delay between each transmit node and the receive node is time-varying and must be tracked

and predicted to facilitate passband signal alignment and coherent transmission. Several recent papers have analyzed the performance of distributed beamforming and distributed nullforming subject to independent oscillator dynamics [5], [8]–[10]. Other than [5], this prior work has primarily focused on the case when the propagation channels are time-invariant or slowly-varying with respect to the oscillator dynamics. Although kinematic effects were studied in [5], the model did not account for the effect of acceleration on the frequency of crystal oscillators as described in [11]. All of this prior work assumed a conventional receiver-coordinated scenario in which the effective channels are tracked using only periodic feedback from the receive node.

This paper analyzes the performance of coherent distributed transmission in a MISO system with independent clock dynamics and time-varying propagation channels. Each propagation channel is assumed to be single-path and its time variations are assumed to be caused by independent kinematics at each transmit node. The receive node is assumed to be stationary. Our analysis accounts for:

- 1) The effect of independent oscillators at each node in the system.
- 2) The effect of acceleration at transmit node  $i$  on the frequency of the oscillator at node  $i$  [11].
- 3) The effect of displacement at transmit node  $i$  on the propagation delay of signals from transmit node  $i$  to the receive node

We develop a continuous-time three-state model describing the combined time offset and propagation delay, normalized rate/frequency offset, and acceleration dynamics between transmit node  $i$  and the receive node. This model is characterized by three parameters corresponding to the short-term oscillator stability, long-term oscillator stability, and kinematic stability. The continuous-time model is then discretized to facilitate tracking with a Kalman filter.

Numerical methods are used to compare the performance of the MISO system in two scenarios: (i) the conventional receiver-coordinated scenario where the combined time offsets and propagation delays are tracked only through periodic feedback of estimates from the receive node and (ii) a scenario where, in addition to the periodic time offset feedback, each receive node also observes measurements from a local accelerometer. This could be achieved, for example, by equipping each transmit node with an inertial measurement unit (IMU). Both time offset feedback and local accelerometer measurements are assumed to be periodic, but the local accelerometer measurements are assumed to be available much more frequently than feedback from the receive node. Numerical results show that local accelerometer measurements can significantly improve the performance of time offset tracking, consequently improving coherence for distributed transmit beamforming and distributed transmit nullforming and also potentially allowing for reduced feedback rates with respect to the conventional receiver-coordinated feedback-only approach.

## II. SYSTEM MODEL

Each node in the system shown in Fig. 1 is assumed to possess a single antenna. All forward link channels are modeled as single-path with identical gain and the time-varying propagation delay of the channel from transmit node  $i$  to the receive node is denoted as  $\psi_i(t)$  with units of seconds for  $i = 1, \dots, N$ .

We assume a protocol in which each transmit node periodically sends a sounding signal at known time (in the transmit node's local timebase) and the time-of-arrival of this signal is estimated at the receive node (in the receive node's local timebase). The receive node estimates the combined time offset and propagation delay of each of the transmit nodes and provides feedback to the transmit nodes to facilitate channel tracking, passband signal alignment, and distributed coherent transmission. As discussed in [5], [8]–[10], the transmit nodes can use Kalman filters to optimally combine this feedback with previously received feedback to generate minimum mean squared error (MMSE) predictions and facilitate coherent transmission between feedback updates.

The time-varying time offset and normalized rate/frequency offset between transmit node  $i$  and the receive node (as observed at the receive node) can be written as

$$\delta_{i,1}(t) = x_{i,1}(t) + \psi_i(t) - x_{0,1}(t) \quad (\text{time offset}) \quad (1)$$

$$\delta_{i,2}(t) = x_{i,2}(t) + \dot{\psi}_i(t) - x_{0,2}(t) \quad (\text{frequency offset}) \quad (2)$$

where  $x_{i,1}(t)$  and  $x_{i,2}(t)$  denote the clock offset and normalized clock rate offsets at node  $i$ , respectively, both with respect to some reference, and where we have adopted the convention that the receiver is node 0. To be clear, the ‘‘time offset’’  $\delta_{i,1}(t)$  includes both the relative clock offset  $x_{i,1}(t) - x_{0,1}(t)$  and the propagation delay  $\psi_i(t)$ . Similarly, the ‘‘frequency offset’’  $\delta_{i,2}(t)$  includes both the relative clock rate offset  $x_{i,2}(t) - x_{0,2}(t)$  and propagation effects in  $\dot{\psi}_i(t)$ . The following sections develop dynamic models for each of the constituent components in these expressions.

### A. Clock Dynamics

The independent local oscillator at each node in the system behaves stochastically, causing time variations the each effective channel from transmit node  $i$  to the receive node. Based on the two-state models in [12], [13], we can define the state of the oscillator at node  $i$  as

$$\mathbf{x}_i(t) = \begin{bmatrix} x_{i,1}(t) \\ x_{i,2}(t) \end{bmatrix} \quad (3)$$

where  $x_{i,1}(t)$  is a time offset with units of seconds and  $x_{i,2}(t)$  is a rate or frequency offset with units of sec/sec (dimensionless), both with respect to some nominal reference. The continuous-time state update equation is given as

$$\dot{\mathbf{x}}_i(t) = \begin{bmatrix} 0 & 1 \\ 0 & 0 \end{bmatrix} \mathbf{x}_i(t) + \boldsymbol{\xi}_i(t) \quad (4)$$

where  $\boldsymbol{\xi}_i(t) = [\xi_{i,1}(t), \xi_{i,2}(t)]^\top$  and where  $\xi_{i,1}(t)$  has units of sec/sec (dimensionless) and  $\xi_{i,2}(t)$  has units of 1/sec. The white process noise  $\boldsymbol{\xi}_i(t)$  is distributed as

$$\boldsymbol{\xi}_i(t) \sim \mathcal{N}(0, \mathbf{Q}) \quad (5)$$

with  $\mathbf{Q} = \text{diag}(q_1, q_2)$  and with  $q_1$  a parameter with units of seconds corresponding to the short-term stability of the oscillator and  $q_2$  a parameter with units of 1/sec corresponding to the long-term stability of the oscillator. We assume all oscillators in the system to have the same  $q_1$  and  $q_2$  parameters. Typical values for short-term and long-term stability parameters for different classes of oscillators can be found in [14].

### B. Effect of Acceleration on Oscillator Frequency

It is well-known that, due to the mechanical nature of crystal oscillators, acceleration applied to a crystal oscillator causes a shift in the oscillator frequency [11]. We assume this effect to be additive with the frequency offsets caused by the non-kinematic clock dynamics as described in the previous section.

To facilitate exposition, we assume the one-dimensional kinematic model illustrated in Fig. 2. The displacement from node  $i$  to the receiver is denoted as  $d_i(t)$  with units of meters. Denoting the acceleration on node  $i$  is  $a_i(t) = \ddot{d}_i(t)$ , the results in [11] imply that the frequency offset caused by acceleration at node  $i$  can be expressed as

$$x_{i,2}(t) = \gamma \ddot{d}_i(t) = \gamma a_i(t) \quad (6)$$

where  $\gamma$  is the oscillator acceleration sensitivity parameter with units of  $\text{sec}^2/\text{m}$ . Typical values for the oscillator acceleration sensitivity parameter are described in [11] and are usually on the order of  $10^{-10} \text{ sec}^2/\text{m}$ . We assume  $\gamma$  is known although this parameter may need to be estimated and/or calibrated in practice. Taking another derivative, we can write

$$\dot{x}_{i,2}(t) = \gamma \dot{a}_i(t) = \gamma j_i(t) \quad (7)$$

where  $j_i(t)$  is the derivative of the acceleration at node  $i$  sometimes called the ‘‘jerk’’ [15].

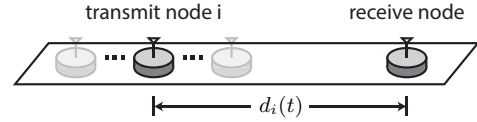


Fig. 2. One dimensional kinematics model with time-varying displacement  $d_i(t)$ .

### C. Effect of Displacement on Propagation Delay

Referring to Fig. 2 and assuming a single-path channel from transmit node  $i$  to the receive node, the propagation delay from node  $i$  to the receiver is given as

$$\psi_i(t) = \frac{d_i(t)}{c} \quad (8)$$

where  $c$  is the speed of light. We can take two derivatives to write

$$\ddot{\psi}_i(t) = \frac{a_i(t)}{c}. \quad (9)$$

This equation is consistent with the usual results for non-relativistic Doppler shifts. We can further define the propagation state

$$\mathbf{z}_i(t) = \begin{bmatrix} \psi_i(t) \\ \dot{\psi}_i(t) \end{bmatrix}. \quad (10)$$

It follows that

$$\dot{\mathbf{z}}_i(t) = \begin{bmatrix} 0 & 1 \\ 0 & 0 \end{bmatrix} \mathbf{z}_i(t) + \begin{bmatrix} 0 \\ \frac{1}{c} \end{bmatrix} a_i(t). \quad (11)$$

### D. Complete Continuous-Time Model

We define the state

$$\boldsymbol{\delta}_i(t) = \begin{bmatrix} x_{i,1}(t) + \psi_i(t) - x_{0,1}(t) \\ x_{i,2}(t) + \dot{\psi}_i(t) - x_{0,2}(t) \\ a_i(t) \end{bmatrix}. \quad (12)$$

Note that the first and second terms of this state vector are the time offset (seconds) and normalized rate/frequency offset (dimensionless), respectively, of node  $i$  as observed at the receive node

through the time-varying propagation delay  $\psi_i(t)$ . Unlike the time and frequency offsets with respect to an unknown reference clock, these offsets are observable.

Using the results from the previous sections, we can write

$$\dot{\delta}_i(t) = \begin{bmatrix} 0 & 1 & 0 \\ 0 & 0 & \frac{1}{c} \\ 0 & 0 & 0 \end{bmatrix} \delta_i(t) + \begin{bmatrix} 1 & 0 & -1 & 0 & 0 \\ 0 & 1 & 0 & -1 & \gamma \\ 0 & 0 & 0 & 0 & 1 \end{bmatrix} \begin{bmatrix} \xi_i(t) \\ \xi_0(t) \\ j_i(t) \end{bmatrix} \quad (13)$$

$$= \mathbf{A}\delta_i(t) + \mathbf{B}\boldsymbol{\eta}_i(t) \quad (14)$$

If we assume the kinematics follow a white-noise jerk model with  $E[j_i(t)j_i(t+\tau)] = q_3\delta(\tau)$  where  $q_3$  has units of  $\text{m}^2/\text{sec}^5$ , then the white process noise  $\boldsymbol{\eta}_i(t)$  is distributed as

$$\boldsymbol{\eta}_i(t) \sim \mathcal{N}(0, \bar{\mathbf{Q}}) \quad (15)$$

with  $\bar{\mathbf{Q}} = E[\boldsymbol{\eta}_i(t)\boldsymbol{\eta}_i^\top(t)] = \text{diag}(q_1, q_2, q_1, q_2, q_3)$ .

### E. Complete Discrete-Time Model

To facilitate tracking with a Kalman filter, this section derives a discrete-time model from the continuous-time model developed in the previous section. The continuous-time transition matrix can be computed as

$$\Phi(t) = e^{\mathbf{A}t} = \begin{bmatrix} 1 & t & \frac{t^2}{2c} \\ 0 & 1 & \frac{t}{c} \\ 0 & 0 & 1 \end{bmatrix}. \quad (16)$$

Let  $T$  denote the sampling period. Using standard methods to convert a continuous-time system to a discrete-time system, e.g., [16], we have a discrete-time state update given as

$$\delta_i[k+1] = \Phi(T)\delta_i[k] + \mathbf{u}_i[k] \quad (17)$$

with

$$\mathbf{u}_i[k] = \int_{kT}^{(k+1)T} \Phi((k+1)T - \tau) \mathbf{B}\boldsymbol{\eta}_i(\tau) d\tau. \quad (18)$$

Note that  $\mathbf{u}_i[k]$  is Gaussian distributed with zero mean since it is a linear function of  $\boldsymbol{\eta}_i(\tau)$  which is Gaussian and zero mean. The discrete-time process noise covariance matrix requires computing

$$\mathbf{C}(T) = \int_0^T \Phi(T - \tau) \mathbf{B}\bar{\mathbf{Q}}\mathbf{B}^\top \Phi^\top(T - \tau) d\tau. \quad (19)$$

Since

$$\mathbf{B}\bar{\mathbf{Q}}\mathbf{B}^\top = \begin{bmatrix} 2q_1 & 0 & 0 \\ 0 & 2q_2 + \gamma^2 q_3 & \gamma q_3 \\ 0 & \gamma q_3 & q_3 \end{bmatrix} \quad (20)$$

and

$$\Phi(T - \tau) = \begin{bmatrix} 1 & T - \tau & \frac{(T - \tau)^2}{2c} \\ 0 & 1 & \frac{T - \tau}{c} \\ 0 & 0 & 1 \end{bmatrix} \quad (21)$$

it can be shown that

$$\mathbf{C}(T) = \int_0^T \sum_{\ell=0}^4 \mathbf{X}_\ell (T - \tau)^\ell d\tau \quad (22)$$

$$= \mathbf{X}_0 T + \mathbf{X}_1 \frac{T^2}{2} + \mathbf{X}_2 \frac{T^3}{3} + \mathbf{X}_3 \frac{T^4}{4} + \mathbf{X}_4 \frac{T^5}{5} \quad (23)$$

where each  $\mathbf{X}_\ell$  is a symmetric  $3 \times 3$  matrix that is only a function of  $c$ ,  $\gamma$ ,  $q_1$ ,  $q_2$ , and  $q_3$  (not a function of  $T$  or  $\tau$ ). Some linear algebra

results in

$$\mathbf{X}_0 = \begin{bmatrix} 2q_1 & 0 & 0 \\ 0 & 2q_2 + \gamma^2 q_3 & \gamma q_3 \\ 0 & \gamma q_3 & q_3 \end{bmatrix}, \quad (24)$$

$$\mathbf{X}_1 = \begin{bmatrix} 0 & 2q_2 + \gamma^2 q_3 & \gamma q_3 \\ 2q_2 + \gamma^2 q_3 & \frac{2\gamma q_3}{c} & \frac{q_3}{c} \\ \gamma q_3 & \frac{q_3}{c} & 0 \end{bmatrix}, \quad (25)$$

$$\mathbf{X}_2 = \begin{bmatrix} 2q_2 + \gamma^2 q_3 & \frac{3\gamma q_3}{2c} & \frac{q_3}{2c} \\ \frac{3\gamma q_3}{2c} & \frac{q_3}{c^2} & 0 \\ \frac{q_3}{2c} & 0 & 0 \end{bmatrix}, \quad (26)$$

$$\mathbf{X}_3 = \begin{bmatrix} \frac{\gamma q_3}{c} & \frac{q_3}{2c^2} & 0 \\ \frac{q_3}{2c^2} & 0 & 0 \\ 0 & 0 & 0 \end{bmatrix}, \text{ and} \quad (27)$$

$$\mathbf{X}_4 = \begin{bmatrix} \frac{q_3}{4c^2} & 0 & 0 \\ 0 & 0 & 0 \\ 0 & 0 & 0 \end{bmatrix}. \quad (28)$$

Hence, the discrete-time dynamics are fully characterized by the initial state  $\delta_i[0]$ , the time-invariant state update matrix  $\mathbf{F} = \Phi(T)$ , and the discrete-time process noise  $\mathbf{u}_i(t) \sim \mathcal{N}(0, \mathbf{C}(T))$  with covariance  $\mathbf{C}(T)$  from (22)–(28).

### F. Observation Model

At each sampling instant  $t = kT$ , transmit node  $i$  receives a noisy observation of the acceleration state from its local accelerometer. At less frequent sampling instances  $t = kT_f$  with  $T_f = MT$  and  $M$  an integer greater than one, transmit node  $i$  receives feedback from the receive node corresponding to a noisy estimate of the time offset state. We assume no estimates are made of the normalized rate/frequency state. The feedback period is denoted as  $T_f$ . Assuming zero latency in the feedback from the receive node, the observation model at node  $i$  can be written as

$$\mathbf{y}_i[k] = \mathbf{H}[k]\delta_i[k] + \mathbf{w}_i[k] \quad (29)$$

where

$$\mathbf{H}[k] = \begin{cases} \begin{bmatrix} 0 & 0 & 0 \\ 0 & 0 & 1 \\ 1 & 0 & 0 \end{bmatrix} & \frac{kT}{T_f} \text{ is not an integer} \\ \begin{bmatrix} 0 & 0 & 0 \\ 0 & 0 & 1 \\ 0 & 0 & 1 \end{bmatrix} & \frac{kT}{T_f} \text{ is an integer} \end{cases} \quad (30)$$

and where  $\mathbf{w}_i[k]$  corresponds to measurement noise. It is reasonable to assume the noise in the accelerometer measurements is independent of the noise in the time offset estimates at the receive node. Hence

$$\mathbf{w}_i[k] \sim \mathcal{N}(0, \mathbf{R}) \quad (31)$$

with  $\mathbf{R} = \text{diag}(r_1, r_2)$ . We assume these measurement noise parameters are identical for all nodes in the system.

Note that the  $r_1$  measurement noise parameter specifies the variance of the time offset measurements at the receive node (which are subsequently fed back over an error-free link to the transmit nodes to facilitate tracking). It is well-known, e.g. [17, p.55], that the Cramer-Rao lower bound (CRLB) for delay estimation of signals observed in additive white Gaussian noise (AWGN) is inversely proportional to the signal-to-noise ratio (SNR) and the mean squared bandwidth of the signal. The analysis leading to this bound, however, assumes a baseband signal is processed to estimate the time offset. Weiss and Weinstein [18], [19] showed that *passband* signal delay estimation performance also improves with carrier frequency when the SNR exceeds a certain threshold. Intuitively, above this SNR threshold, the presence of the carrier in the passband signal provides

additional detail in the correlator output that can be used to refine delay estimates to a fraction of a carrier period.

As an example, in the case of a pre-integration SNR of 10 dB, bandwidth  $B = 50$  MHz, waveform duration  $T = 10 \mu\text{s}$ , and carrier frequency  $\omega_0 = 2\pi \cdot 1$  GHz, the passband CRLB implies that RMS delay estimation errors can be as small as approximately 4 ps. Experimental results reported in [20] with similar signaling parameters in an outdoor environment and with off-the-shelf hardware yielded RMS delay estimation errors of less than 10 ps.

The  $r_2$  measurement noise parameter specifies the variance of the noise in the accelerometer measurements. We have assumed here a simplified model for the accelerometer that ignores any amplitude nonlinearities and/or bias effects. The value of  $r_2$  depends on accelerometer noise specifications and the measurement bandwidth. As an example, the Analog Devices ADXL103/ADXL203 accelerometer datasheet [21] has a noise density specification of  $110 \mu\text{g}/\sqrt{\text{Hz}}$ . If a single-pole anti-aliasing filter with bandwidth  $\text{BW}$  Hz is used to limit the noise prior to sampling, the RMS accelerometer noise can be calculated as [21]

$$\text{RMSnoise} \approx \left(110 \frac{\mu\text{g}}{\sqrt{\text{Hz}}}\right) \left(\sqrt{\text{BW} \cdot 1.6}\right) \left(9.8 \cdot 10^{-6} \frac{\text{m/s}^2}{\mu\text{g}}\right) \quad (32)$$

with units of  $\text{m/s}^2$  and where the factor of 1.6 is due to the rolloff of the single-pole anti-aliasing filter. For example, with an accelerometer sampling period of  $T = 0.01$ , we can set  $\text{BW} = 50$  Hz and compute  $\text{RMSnoise} \approx 9.64 \times 10^{-3} \text{ m/s}^2$ . The  $r_2$  parameter then follows as  $r_2 = (\text{RMSnoise})^2$ . In this example, we have  $r_2 \approx 9.3 \times 10^{-5} \approx 1 \times 10^{-4} \text{ m}^2/\text{s}^4$ .

### III. NUMERICAL RESULTS

In this section, we demonstrate the performance advantages of using local accelerometer measurements to improve the effective tracking performance and, consequently, improve the coherence of the distributed transmission system. Table I lists the parameters for all of the numerical results in this section.

TABLE I  
PARAMETERS FOR NUMERICAL RESULTS.

Parameter	Value	Units	Meaning
$q_1$	$10^{-22}$	sec	oscillator short-term stability
$q_2$	$10^{-23}$	1/sec	oscillator long-term stability
$q_3$	$4 \cdot 10^{-2}$	$\text{m}^2/\text{sec}^5$	white noise jerk process noise intensity
$\gamma$	$10^{-10}$	$\text{sec}^2/\text{m}$	oscillator sensitivity to acceleration
$r_1$	$4 \cdot 10^{-24}$	$\text{sec}^2$	time offset measurement noise variance
$r_2$	$10^{-4}$	$\text{m}^2/\text{sec}^4$	accelerometer measurement variance
$T$	0.01	sec	sampling period for accelerometer measurements
$T_f$	0.50	sec	sampling period for time offset measurements (feedback)
$\omega_0$	$2\pi \cdot 900 \cdot 10^6$	rad/sec	nominal carrier frequency

The oscillator stability parameters were chosen to be similar to the “good” XO parameters described in [14]. The white noise jerk process noise intensity was chosen so that the changes in the acceleration over the sampling period  $T$  were on the order of  $\sqrt{Tq_3} = 0.02 \text{ m/sec}^2$ . The oscillator sensitivity parameter was chosen according to typical values described in [11]. The measurement noise parameters depend

on various factors such as the integrated SNR and the quality of the accelerometer. We have assumed here sufficient SNR so that the time offset estimation performance follows the Weiss-Weinstein bounds for passband signals [18], [19] and are on the order of picoseconds as has been experimentally demonstrated in [22]. The accelerometer measurement variance  $r_2$  was set according to the example calculation based on the ADXL103/ADXL203 accelerometer [21] in the previous section.

Fig. 3 shows the tracking performance of a Kalman filter channel tracker with and without local accelerometer observations using the parameters in Table I at the 900 MHz nominal carrier frequency averaged over 1000 independent realizations of the clock and kinematic processes. These results are shown in RMS phase prediction error (degrees) versus time. At times  $t = 0, 0.5, 1.0, \dots$ , the transmit node receives feedback from the receive node and we see the RMS phase prediction error is small when this feedback is received. In the case without local accelerometer observations, the kinematics and clock dynamics cause the phase predictions to quickly become inaccurate. For the case with local accelerometer observations, the transmitters use these observations (received at times  $t = 0, 0.01, 0.02, \dots$ ) to better predict the combined time offset and propagation delay and reduce the RMS phase prediction error between feedback periods. While the local accelerometer measurements don’t account for the clock dynamics, they do provide useful information about the kinematic effects on the local clock frequency and changes in the propagation delay.

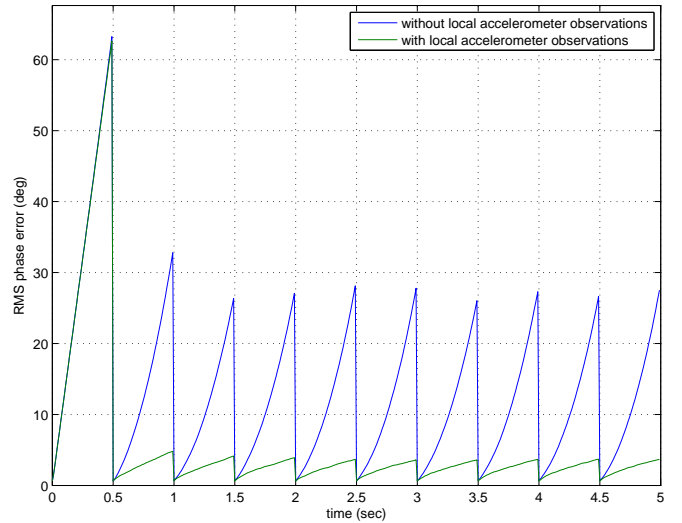


Fig. 3. RMS phase prediction error in degrees versus time with and without local accelerometer observations.

Fig. 4 shows the beamforming gain of an  $N = 10$  node distributed beamformer with each transmit node in the system using a Kalman filter to track and predict the effective channel dynamics. The performance is compared with and without local accelerometer observations using the parameters in Table I at the 900 MHz nominal carrier frequency averaged over 1000 independent realizations of the clock and kinematic processes and assume identical channel magnitudes from each transmit node to the receive node. Under this assumption, it has been shown [10] that the average beamforming gain with respect to incoherent transmission is related to the variance of the phase

prediction errors according to

$$E[\text{beamforming gain}] = Ne^{-\sigma_\phi^2(t_p)} + (1 - e^{-\sigma_\phi^2(t_p)}) \quad (33)$$

where  $\sigma_\phi^2(t_p)$  denotes the phase prediction variance at prediction time  $t_p$  from the last feedback update. In this case, since the ideal beamforming gain of an  $N = 10$  node array is 10 dB, these results show that local accelerometer observations allow the distributed transmit array to maintain performance almost indistinguishable from an ideal beamformer for  $t > 0.5$ . If local accelerometer observations are not available, the kinematic effects are poorly tracked and the distributed array loses approximately 1 dB of beamforming gain just prior to receiving a feedback update from the receiver.

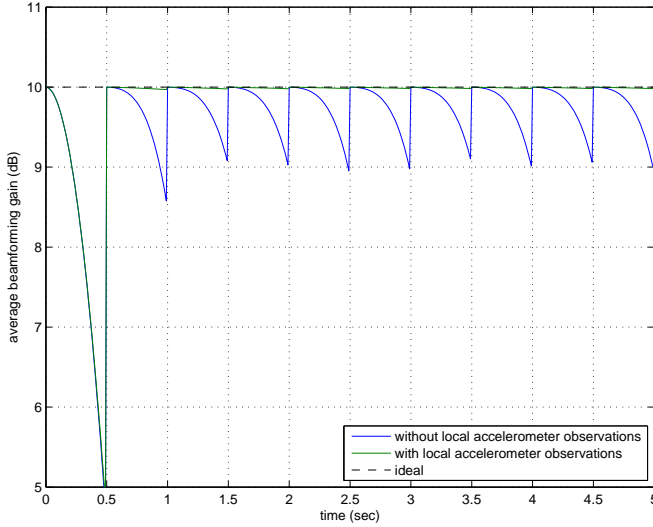


Fig. 4. Average beamforming gain with respect to incoherent transmission in dB for an  $N = 10$  node transmit cluster versus time with and without local accelerometer observations.

Fig. 5 shows the *nullforming* gain of an  $N = 10$  node distributed beamformer with each transmit node in the system using a Kalman filter to track and predict the effective channel dynamics under the same assumptions as the previous results. The goal in this case is to minimize the power at the receiver. Nullforming is used, for example, in cognitive radio underlay networks to avoid interfering with primary users [23]. In [10], it was shown that the average nullforming gain with respect to incoherent transmission is related to the variance of the phase prediction errors according to

$$E[\text{nullforming gain}] = 1 - e^{-\sigma_\phi^2(t_p)}. \quad (34)$$

where  $\sigma_\phi^2(t_p)$  denotes the phase prediction variance at prediction time  $t_p$  from the last feedback update. These results show that accelerometer observations allow for nulls better than 20 dB below incoherent transmission whereas a system without accelerometer observations has nulls that are often less than 10 dB below incoherent transmission. Intuitively, the large performance advantage of the system with accelerometer observations in this example is due to the fact that nulls tend to be more sensitive to phase prediction errors than beams. By using local accelerometer measurements, the variance of the phase prediction errors is significantly reduced and the nullforming performance is significantly improved.

It is also of interest to understand how accelerometer measurements can be used to reduce feedback overhead in distributed transmission systems. Fig. 6 shows the achievable reduction in the feedback update

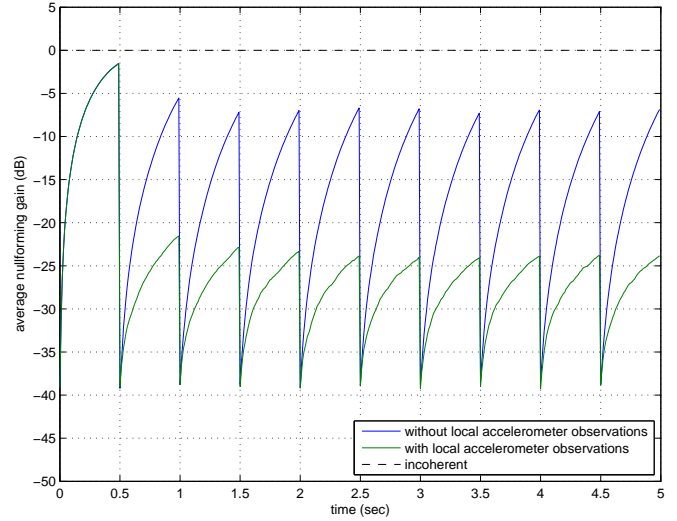


Fig. 5. Average nullforming gain with respect to incoherent transmission in dB for an  $N = 10$  node transmit cluster versus time with and without local accelerometer observations.

rate  $\frac{1}{T_f}$  of a system *with* accelerometer measurements achieving equivalent performance of a conventional receiver-coordinated system *without* accelerometer measurements. To be specific, we denote the feedback rate with and without accelerometer measurements as  $\frac{1}{T_f^{(\text{wam})}}$  and  $\frac{1}{T_f^{(\text{woam})}}$ , respectively. For a fixed value of  $T_f^{(\text{woam})}$ , we compute the performance of the conventional receiver-coordinated system without accelerometer measurements by temporally averaging the Kalman filter RMS phase prediction errors after the 20<sup>th</sup> observation and before the 21<sup>st</sup> observation (similar results are obtained by considering beamforming or nullforming gain as the performance metric). Setting  $T_f^{(\text{wam})} = T_f^{(\text{woam})}$  and running the same experiment on the system with accelerometer measurements results in improved performance (reduced temporally-averaged RMS phase prediction errors). Keeping the accelerometer measurement period  $T = 0.01$  fixed, we then decrease the feedback update rate  $\frac{1}{T_f^{(\text{wam})}}$  until the system with accelerometer measurements achieves identical performance to the conventional receiver-coordinated system without accelerometer measurements with feedback update rate  $\frac{1}{T_f^{(\text{woam})}}$ .

The results in Fig. 6 plot the reduction in the feedback rate  $\frac{1/T_f^{(\text{woam})}}{1/T_f^{(\text{wam})}}$  versus the feedback rate without accelerometer compensation  $\frac{1}{T_f^{(\text{woam})}}$ . For example, a value of two corresponds to the case where the system with accelerometer compensation can achieve the same performance as a system without accelerometer compensation by reducing the feedback rate by a factor of two. These results show how a system with accelerometer measurements can achieve the same performance as a system without accelerometer measurements with significantly less feedback overhead. Larger feedback rate reductions occur in this example when the feedback rate in the conventional receiver-coordinated system is low.

#### IV. CONCLUSION

This paper developed a model and analyzed the performance of distributed coherent transmission in a MISO communication system with time-varying propagation channels. The analysis accounted for the effects of independent clock dynamics as well as the effects of independent kinematics on the frequency of each transmit node

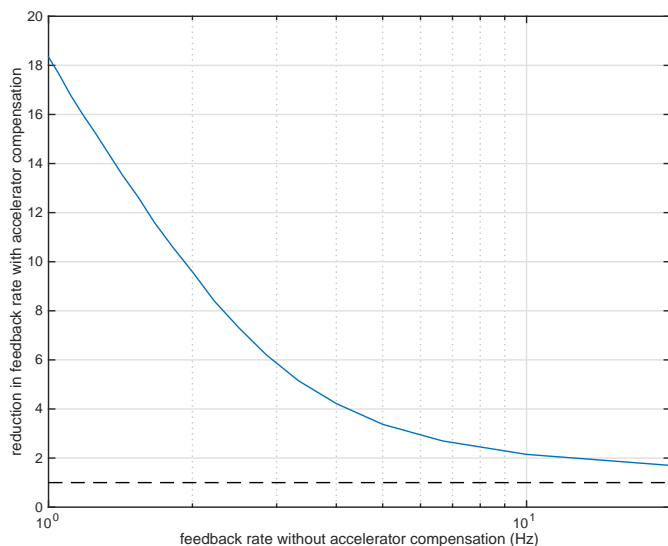


Fig. 6. Reduction in feedback rate for a system with accelerometer measurements achieving equivalent tracking performance of a conventional receiver-coordinated system without accelerometer measurements. The accelerometer measurement period was fixed at  $T = 0.01$  seconds.

and the delay of each propagation channel. Two scenarios were considered: (i) the conventional receiver-coordinated scenario where the time offsets are tracked only through periodic feedback from the receive node and (ii) an accelerometer-assisted scenario where, in addition to the periodic time offset feedback, each receive node also observes measurements from a local accelerometer. Numerical results demonstrated that local accelerometer measurements can improve the ability of each node to track its time offset with respect to the receive node, consequently improving coherence for distributed transmit beamforming and distributed transmit nullforming and also allowing for reduced feedback rates with respect to the conventional feedback-only approach.

The analysis in this paper was simplified by the one-dimensional kinematics assumption as depicted in Fig. 2. In general, with two-dimensional or three-dimensional kinematics, the orientation of the accelerometer with respect to the sensitivity axis of the oscillator [11] and the direction of the propagation channel may be unknown and possibly time-varying. Since the orientation affects elements of the state update matrix  $F$  and the process noise covariance  $C(T)$ , it is critical to generate accurate estimates of these parameters to facilitate optimal tracking and coherent transmission. Methods for accelerometer compensation with two-dimensional and three-dimensional kinematics would be an interesting extension to this work.

## REFERENCES

- [1] R. Mudumbai, G. Barriac, and U. Madhoo, "On the feasibility of distributed beamforming in wireless networks," *IEEE Trans. on Wireless Communications*, vol. 6, no. 5, pp. 1754–1763, May 2007.
- [2] R. Mudumbai, D. Brown, U. Madhoo, and H. Poor, "Distributed transmit beamforming: challenges and recent progress," *Communications Magazine, IEEE*, vol. 47, no. 2, pp. 102–110, February 2009.
- [3] R. Preuss and D. Brown, "Retrodirective distributed transmit beamforming with two-way source synchronization," in *Information Sciences and Systems (CISS), 2010 44th Annual Conference on*, March 2010, pp. 1–6.
- [4] R. Preuss and D.R. Brown III, "Two-way synchronization for coordinated multi-cell retrodirective downlink beamforming," *IEEE Trans. on Signal Processing*, vol. 59, no. 11, pp. 5415–27, Nov. 2011.

- [5] D. Brown III, P. Bidigare, and U. Madhoo, "Receiver-coordinated distributed transmit beamforming with kinematic tracking," in *Acoustics, Speech and Signal Processing (ICASSP), 2012 IEEE International Conference on*, Mar. 2012, pp. 5209–5212.
- [6] K. Zarifi, S. Affes, and A. Ghayeb, "Collaborative null-steering beamforming for uniformly distributed wireless sensor networks," *IEEE Trans. on Signal Processing*, vol. 58, no. 3, pp. 1889–1903, Mar. 2010.
- [7] D.R. Brown III and U. Madhoo, "Receiver-coordinated distributed transmit nullforming with channel state uncertainty," in *Conf. Inf. Sciences and Systems (CISS2012)*, Mar. 2012.
- [8] D.R. Brown III, P. Bidigare, S. Dasgupta, and U. Madhoo, "Receiver-coordinated zero-forcing distributed transmit nullforming," in *Statistical Signal Processing Workshop (SSP), 2012 IEEE*, Aug. 2012, pp. 269–272.
- [9] D. Brown III, R. Mudumbai, and S. Dasgupta, "Fundamental limits on phase and frequency tracking and estimation in drifting oscillators," in *Acoustics, Speech and Signal Processing (ICASSP), 2012 IEEE International Conference on*, Mar. 2012, pp. 5225–5228.
- [10] D.R. Brown III and R. David, "Receiver-coordinated distributed transmit nullforming with local and unified tracking," in *Proc. of the 39th International Conf. on Acoustics, Speech, and Signal Processing (ICASSP2014)*, Florence, Italy, May 4-9 2014.
- [11] R. Filler, "The acceleration sensitivity of quartz crystal oscillators: a review," *Ultrasonics, Ferroelectrics, and Frequency Control, IEEE Transactions on*, vol. 35, no. 3, pp. 297–305, May 1988.
- [12] L. Galleani, "A tutorial on the 2-state model of the atomic clock noise," *Metrologia*, vol. 45, no. 6, pp. S175–S182, Dec. 2008.
- [13] G. Giorgi and C. Narduzzi, "Performance analysis of kalman filter-based clock synchronization in IEEE 1588 networks," in *International IEEE Symposium on Precision Clock Synchronization for Measurement, Control, and Communication*, October 12-16 2009, pp. 1–6.
- [14] W. Klepczynski and P. Ward, "Frequency stability requirements for narrow band receivers," in *32nd Annual Precise Time and Time Interval Meeting*, November 2000.
- [15] Y. Bar-Shalom, X. R. Li, and T. Kirubarajan, *Estimation with Applications to Tracking and Navigation*. John Wiley and Sons, 2001.
- [16] C.-T. Chen, *Linear System Theory and Design*. Oxford University Press, 1999.
- [17] S. M. Kay, *Fundamentals of Statistical Signal Processing Volume I: Estimation Theory*. Upper Saddle River, NJ: Prentice Hall, 1993.
- [18] A. Weiss and E. Weinstein, "Fundamental limitations in passive time delay estimation—part i: Narrow-band systems," *Acoustics, Speech and Signal Processing, IEEE Transactions on*, vol. 31, no. 2, pp. 472–486, April 1983.
- [19] E. Weinstein and A. Weiss, "Fundamental limitations in passive time-delay estimation—part ii: Wide-band systems," *Acoustics, Speech and Signal Processing, IEEE Transactions on*, vol. 32, no. 5, pp. 1064–1078, October 1984.
- [20] P. Bidigare, S. Pruessing, D. Raeman, D. Scherber, U. Madhoo, and R. Mudumbai, "Initial over-the-air performance assessment of ranging and clock synchronization using radio frequency signal exchange," in *IEEE Stat. Signal Processing Workshop (SSP)*, Aug. 2012, pp. 273–276.
- [21] "Analog Devices ADXL103/ADXL203 Precision Dual-Axis iMEMS Accelerometer Datasheet," 2014. [Online]. Available: {[http://www.analog.com/static/imported-files/data\\_sheets/ADXL103\\_203.pdf](http://www.analog.com/static/imported-files/data_sheets/ADXL103_203.pdf)}
- [22] P. Bidigare, M. Oyarzun, D. Raeman, D. Cousins, D. Chang, R. O'Donnell, and D.R. Brown III, "Implementation and demonstration of receiver-coordinated distributed transmit beamforming across an ad-hoc radio network," in *Proc. of the 46th Asilomar Conf. on Signals, Systems, and Computers*, Pacific Grove, CA, November 4-7 2012, pp. 222–226.
- [23] Y. Noam and A. Goldsmith, "Blind null-space learning for mimo underlay cognitive radio with primary user interference adaptation," *Wireless Communications, IEEE Transactions on*, vol. 12, no. 4, pp. 1722–1734, April 2013.